Convolutional Neural Network (CNN) Architecture for Detecting *Fusarium wilt* in Banana Crops Using UAV-Based Multispectral Imaging

Gabriela Zanchetta[1], Fernanda Sayuri Yoshino Watanabe[2], Hideo Araki[3]

[1]São Paulo State University - UNESP, School of Sciences and Technology, Graduate Program of Cartographic Sciences, Presidente Prudente, SP Brazil - gabriela.zanchetta@unesp.br;
[2]São Paulo State University - UNESP, School of Sciences and Technology, Graduate Program of Cartographic Sciences, Presidente Prudente, SP Brazil – fernanda.watanabe@unesp.br;
[3]Federal University of Paraná - UFPR, Department of Geomatic, Curitiba, PR, Brazil - haraki@ufpr.br

Keywords: Remote Sensing, Drone, Deep Learning, Agriculture, Disease Identification, *Fusarium wilt*.

Abstract

Banana crops are highly susceptible to Fusarium wilt, a disease that can cause significant crop losses if not detected early. This study aimed to develop a classification model to detect Fusarium-infected banana plants using multispectral images. The dataset consisted of labeled images categorized into two classes: healthy and diseased (*Fusarium*). A convolutional neural network (CNN) was trained and evaluated, achieving an overall test accuracy of 81.25%. Class-wise evaluation showed a precision of 70%, recall of 100%, and F1 score of 82% for healthy plants, while the diseased class achieved 100% precision, recall of 67%, and F1 score of 80%. These results indicate strong precision performance but highlight the need to improve recall for effective disease monitoring. Comparisons with recent studies show that greater accuracy can be achieved through larger datasets and data augmentation. Following this approach, when other techniques were applied to the network (such as k-fold, class balancing, and spectral index segmentation), the model achieved maximum values (100%) for all evaluated metrics. This research demonstrates the potential of using multispectral images and deep learning for banana disease classification, with improvements focused on expanding the data volume and applying advanced training techniques to increase recall and overall robustness.

1. Introduction

Banana (*Musa* spp.) is one of the most valuable primary agricultural commodities in the world, being one of the most produced and traded crops globally (Ploetz, 2021). According to the Food and Agriculture Organization (FAO) of the United Nations, China is one of the largest banana producers (11.70 million tons) in the world (FAOSTAT, 2023), second only to India (36.61 million tons). Indonesia, Nigeria, Ecuador, Brazil, Philippines, Angola, Guatemala and United Republic of Tanzania are on the list of countries that produce the most bananas, in descending order. Despite increasing production, some producers have been suffering from banana diseases and pests, which are damaging agricultural production. If these diseases are not detected early, therefore, they can lead to increased food insecurity (Chen et al., 2020).

Among the various plant health problems of banana plants, *Fusarium* wilt (also known as Panama disease and banana cancer) stands out (Simmonds, 1996), caused by the fungus *Fusarium oxysporum f. sp. cubense (Foc),* a soil-borne fungus. The lower, most mature leaves on infected plants tend to droop, perish, and frequently tear at the base (Stover, 1962), and yellowing of leaf lamina is common (Ploetz, 2015). Additionally, cracks are seen on the underside along the length of the stem (Denny et al., 2022). This disease brings great challenges to the farmers' economy. Fields with severe infections can suffer up to 100% yield loss, resulting in total crop failure and causes social impacts (Nakkeeran et al., 2021).

The ultimate solution is so far unavailable (Pegg et al., 2019). To control the fungus, field inspections must be frequent and whenever a diseased plant is detected, it must be eliminated (EMBRAPA, 2022). In abandoned fields, the tropical race 4 (TR4) fungus can survive for 40 years (and may be longer) (Stover and Waite, 1954). Besides bananas, other crops also suffer from the fungus, such as tomato (Couteaudier and Alabouvette, 1981), radish (Dang et al., 2020b), bean (Fall et al., 2001), chickpea (Yadav et al., 2023) and cotton seedlings (Zhu et al., 2021). Detecting *Fusarium* is extremely important for reducing labour costs for these crops.

Traditional on-foot inspections have been used for years, yet they are slow and labour-intensive, and cannot be guaranteed, due to the large areas of plantations. So that, remote sensing along with deep learning can contribute to accurate and less arduous evaluations. Although contemporary Convolutional Neural Network (CNN) models typically demand substantial computing resources, researchers have been working to slim down their resource requirements without sacrificing accuracy. For *Fusarium* wilt, studies have used networks such as: GoogleNet (Dang et al., 2020a), ResNet50 (Yan et al., 2023), ResNet152 (Sanga et al., 2020), Inception-V3 (Dang et al., 2020a; Sanga et al., 2020), VGG-16 (Dang et al., 2020a), YOLOv8n (Lin et al., 2025) and RadRGB (Dang et al., 2020b). Also, some studies have adopted spectral indices as model input (Dang et al., 2020b; Zhang et al., 2022).

Remote sensing based on Unmanned Aerial Vehicle (UAV) has seen rapid advancement in recent years, because it allows the acquisition of images in high spatial resolution; can be operated on demand (in specific locations and times); does not depend on pre-determined orbits (as in the case of satellites); and has less atmospheric interference. Multispectral sensors capture nuanced spectral data beyond standard RGB, extending into the red edge and near-infrared (NIR) regions for enhanced analysis. However, researches using with UAV-based multispectral imagery for detection/classification of *Fusarium* are still rare (Ye et al., 2020a, 2020b; Zhang et al., 2022).

Thereby, the aim of this study was to develop a CNN-based classification model capable of distinguishing between healthy

This contribution has been peer-reviewed. The double-blind peer-review was conducted on the basis of the full paper.
https://doi.org/10.5194/isprs-annals-X-3-W4-2025-371-2026

and Fusarium-infected banana plants using multispectral imagery.

2. Materials and Methodology

2.1 Study Area and Instruments

The study was conducted in an area of 18 ha banana crop, located in Long'an County, Guangxi Zhuang Autonomous Region, southern China (Figure 1). The data was extracted from the Science Data Bank (Huichun et al., 2023) and this dataset allows downloading the orthomosaic of the area, which was performed by multispectral images acquired by the MicaSense RedEdge M^{TM} camera (MicaSense, Inc., Seattle, WA, USA) of five spectral bands (Figure 2a): blue (465–485 nm), green (550–570 nm), red (653–673 nm), red edge (712–722 nm) and NIR (800–880 nm), which was embarked on an UAV DJI Phantom 4 (DJI Innovations, Shenzhen, China), presented in the Figure 2b.

The flight height was 120 m, and the Ground Sample Distance (GSD) was 8 cm. Besides of the orthomosaic, the dataset also makes available ground survey data regarding healthy banana plants and those with the presence of banana wilt disease. In total, 80 sample elements were used (40 healthy and 40 with the presence of the disease).

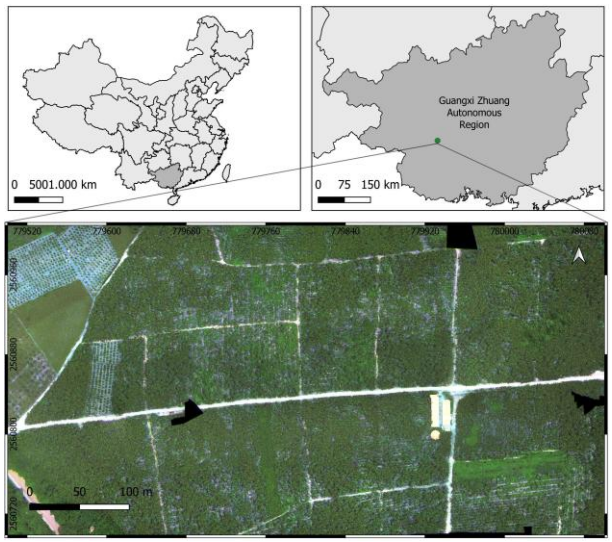

Figure 1. Banana plantation area in Long'an County, Guangxi Zhuang Autonomous Region, southern China.

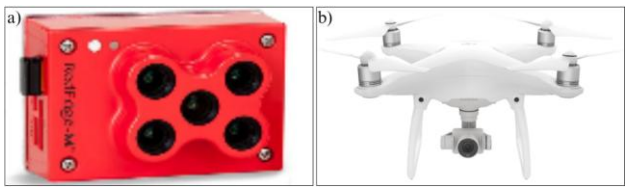

Figure 2., MicaSense RedEdge M^{TM} camera (a), provided by MicaSense Inc., and (b) UAV DJI Phantom 4, provided by DJI Innovations.

For better visualization of the proposed methodology, a flowchart is presented in Figure 3. The workflow includes data acquisition (by UAV multispectral images), image data (38 x 38 pixels), pre-processing (normalization of reflectance values; calculation of spectral indices; simple segmentation by Normalized Difference Vegetation Index – NDVI; resizing the image from 38 x 38 to 64 x 64; data augmentation with rotations, translations, flips, zoom and brightness) model training using a CNN in Google Colaboratory, and evaluation using standard classification metrics, that include: accuracy, precision, recall, F1-score, confusion matrix and Receiver Operating Characteristic (ROC) curve.

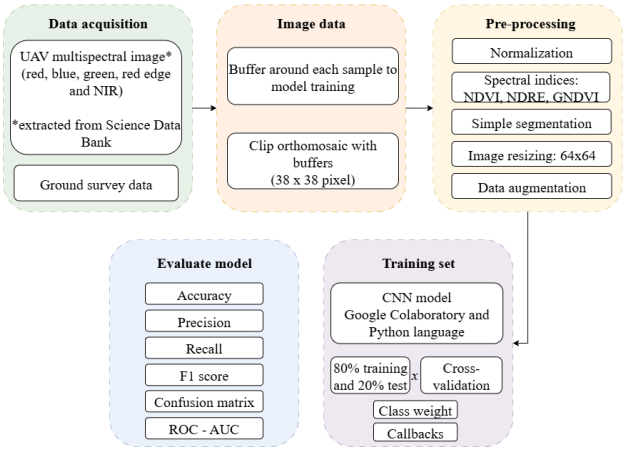

Figure 3. Flowchart illustrating the deep learning pipeline for classifying healthy and disease banana crop.

2.2 Image Data

From the orthomosaic and soil samples made available by the dataset, 3 m x 3 m buffers were extracted (Figure 4), using the QGIS software (Open-Source Geospatial Foundation, Corvallis, United States), which were used for clipping and generation of new images for training and testing the model. Each of these cutouts sought to represent a banana tree and had dimensions of 5, 38, 38, being number of bands, height (pixel) and width (pixel), respectively.

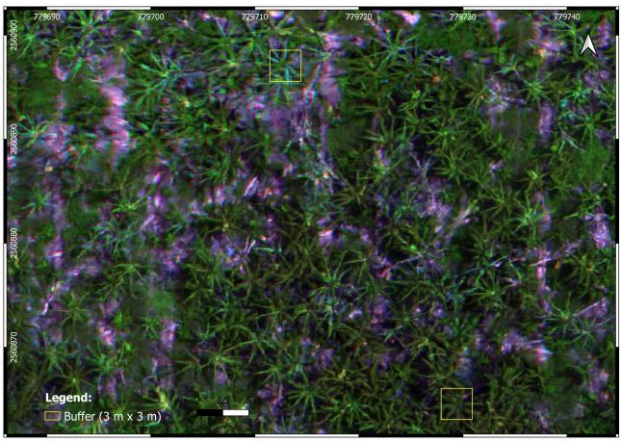

Figure 4. Buffers measuring 3 m x 3 m were extracted from the soil samples.

2.3 Pre-processing and training set

To train the network, different tests were performed to achieve the best model, with the description below for each of them (i, ii, iii):

i. Initially, from the dataset with 80 sample elements, 80% of the samples were used for training and 20% for testing. For this case, no other techniques were applied.

ii. For this test, the stratified k-fold (*StratifiedKFold,* from *scikit-learn*) and data augmentation technique was employed. Data augmentation consists of generating variations of the original images through transformations such as rotation, flipping, and changes in brightness and contrast. Additionally, the implementation incorporates the k-fold cross-validation strategy, which is a widely recognized technique for ensuring that the model generalizes well to unseen data. In this approach, the dataset is divided into k parts (in this case, k = 5), where, in each iteration, one part is used for validation while the remaining parts are used for training. In each fold of cross-validation, we sought the threshold that best separated the classes according to the chosen metric. This ensures that the evaluation reflects the model's actual performance, adapted to the characteristics of each data division.

iii. Here, in addition to k-fold optimization, the segmentation, spectral index, class weight and callbacks techniques were also employed. Vegetation spectral indexes, such as NDVI (Rouse et al., 1974), Normalized Difference Red Edge (NDRE) (Gitelson and Merzlyak, 1996), and Green Normalized Difference Vegetation Index (GNDVI) (Gitelson et al., 1996), are features that utilize different spectral bands to enhance information about vegetation condition. Segmentation is a technique that allows identifying and delimiting areas of interest within an image, facilitating the analysis of specific plant characteristics. In this case, segmentation was performed using a simple approach based on the NDVI index, which helps to distinguish between healthy vegetative areas and those affected by stress. Weight balancing is used to penalize more errors in minority classes. Dropout was applied as a regularization technique (rate = 0.4), which during training randomly deactivates 40% of the layer units, reducing neuron co-adaptation and helping to mitigate overfitting. And the use of *ReduceLROnPlateau* (from *keras*) as a callback to reduce the learning rate when the validation metric plateaus, helping convergence and avoiding loss oscillation.

2.4 Convolutional Neural Network (CNN) Model

Convolutional Neural Network (CNN) is a architecture in deep learning and was introduced in 1989 (LeCun et al., 1989). The basic structure of CNN consists in five layers architecture: input layer (in this case, an image with 5 bands and a dimension of 38 x 38 pixels), convolutional layer, pooling layer, flatten layer and fully connected layer (Figure 5). The input image is passed through a convolutional layer, which uses filters to detect patterns. Using max pooling, these features are downsampled, reducing the spatial dimensions. Then, the feature maps are flattened into a 1D vector. A series of fully connected (dense) layers learn increasingly abstract representations of the image, extracting relevant patterns. Finally, the final dense layer produces the output – classification.

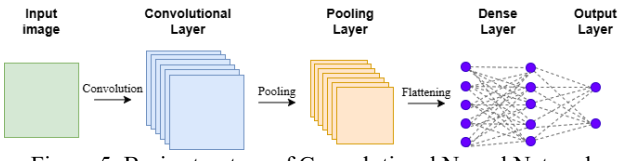

Figure 5. Basic structure of Convolutional Neural Network (CNN): input layer, convolutional layer, pooling layer, flatten layer and fully connected layer.

As mentioned, in this study it was used a CNN, and its details can be seen in Table 1. The value of 25 was chosen for epochs (i) and 50 (ii, iii). In addition, a seed (42) was selected to avoid randomness in the data. Google Colaboratory and Python language were used to develop the network.

Layer Tipe	Details
Convolutional Layer	32 filters, 3×3 kernel, ReLU activation
Max Pooling Layer	2×2 pool size
Flatten Layer	Transforms 2D output to 1D vector
Dense Layer 1	16 neurons, ReLU activation
Dense Layer 2	32 neurons, ReLU activation
Dense Layer 3	64 neurons, ReLU activation
Dense Layer 4	32 neurons, ReLU activation
Output Dense Layer	1 neuron, sigmoid activation (for binary classification)

Table 1. Architecture of the Convolutional Neural Network (CNN) Model for Binary Classification.

2.5 Model Evaluation

The metrics used to determine the overall performance of the model were: accuracy, precision, recall, and F-1 score. These measures are calculated using Equations (1) – (4), respectively. Additionally, a confusion matrix was visualized to see the exact number of true and false positive and negative identification classes. The ROC curve was also calculated using the generated code to verify the model's performance and its discriminatory capacity.

$$Accuracy = \frac{TP + TN}{TP + TN + FP + FN}, \quad (1)$$

$$Precision = \frac{TP}{TP + FP}, \quad (2)$$

$$Recall = \frac{TP}{TP + FN}, \quad (3)$$

$$F1\ Score = \frac{2 \times Precision \times Recall}{Precision + Recall}, \quad (4)$$

where TP = True positive
TN = True negative
FP = False positive
FN = False negative

3. Results and Discussion

The results obtained from applying a convolutional neural network (CNN) to binary classification of *Fusarium* disease are presented in detail below (Table 2), organized into three distinct datasets: (i), (ii), and (iii).

In the first dataset (i), the results show a precision of 0.70 for the "*Healthy*" class and 1.00 for the "*Fusarium*" class, reflecting the model's ability to correctly identify healthy instances, but with a lower ability to detect *Fusarium* infections, evidenced by a recall of 0.67. The F1-score, which considers both precision and recall, was 0.82 for the "*Healthy*" class and 0.80 for "*Fusarium*." The model demonstrated an overall accuracy of 0.81, indicating that, on average, 81% of predictions were correct. The macro and weighted averages for precision and recall were 0.85 and 0.83, respectively, demonstrating a reasonable balance between precision and data recall. The ROC curve obtained an area of 0.89, demonstrating the model's good ability to differentiate between classes.

This contribution has been peer-reviewed. The double-blind peer-review was conducted on the basis of the full paper.
https://doi.org/10.5194/isprs-annals-X-3-W4-2025-371-2026 | © Author(s) 2026. CC BY 4.0 License.

In the second dataset (ii), there was a significant improvement in the metrics. Precision reached 0.93 for "*Healthy*" and 0.97 for "*Fusarium*," while recall also increased, reaching 0.98 for "*Healthy*" and 0.93 for "*Fusarium*." The overall F1-score was 0.95, reflecting robust model performance in both classes. Accuracy was 0.95, reinforcing the CNN's reliability. The macro and weighted averages remained at 0.95, demonstrating consistency in performance metrics across classes. The ROC curve showed an area of 0.97, indicating the model's excellent ability to distinguish between healthy and diseased individuals.

In the third dataset (iii), the results were remarkable, with a precision and recall of 1.00 for both the "*Healthy*" and "*Fusarium*" classes. The F1-score also reached the maximum value of 1.00, demonstrating that the model perfectly classified all instances. Accuracy was also perfect, at 1.00. The macro and weighted averages also showed consistent results of 1.00, reflecting the model's optimal performance across all aspects analyzed. The ROC curve reached an area of 1.00, demonstrating the CNN's complete ability to discriminate between classes.

In summary, the results show a significant improvement in performance metrics across the different datasets when certain techniques were implemented in the model. As seen in (ii), the data augmentation and k-fold techniques already indicated a considerable improvement. But with more techniques employed (such as segmentation from vegetation indices and classweight), the model was able to obtain maximum values for the metrics.

	Precision	Recall	F1-score	Support
Dataset (i)				
Healthy	0.70	1.00	0.82	7
Fusarium	1.00	0.67	0.80	9
Accuracy			0.81	16
Macro average	0.85	0.83	0.81	16
Weighted average	0.87	0.81	0.81	16
ROC: 0.89				
Dataset (ii)				
Healthy	0.93	0.98	0.95	40
Fusarium	0.97	0.93	0.95	40
Accuracy			0.95	80
Macro average	0.95	0.95	0.95	80
Weighted average	0.95	0.95	0.95	80
ROC: 0.97				
Dataset (iii)				
Healthy	1.00	1.00	1.00	40
Fusarium	1.00	1.00	1.00	40
Accuracy			1.00	80
Macro average	1.00	1.00	1.00	80
Weighted average	1.00	1.00	1.00	80
ROC: 1.00				

Table 2. Comprehensive classification report including class-wise precision, recall, F1-score, support, overall accuracy, macro average, and weighted average metrics based in each training set.

The lower recall for the *Fusarium* class (i) highlights a common challenge in disease detection models, particularly when working with limited and imbalanced datasets. As noted in the literature, performance can significantly improve with larger datasets and techniques such as data augmentation and transfer learning. For instance, Yan et al. (2023) reported a boost from 76% to 98% accuracy using ResNet-50 with transfer learning and data augmentation methods. Which we can also see here, from 0.81 to 0.95, and then to 1.00.

Comparatively, our results are quite competitive. Dang et al. (2020a) achieved 91.5% accuracy for *Fusarium* classification in radish using the GoogleNet architecture with smaller image windows. In a follow-up study, Dang et al. (2020b) improved accuracy to 96% using UAV imagery (RGB/NIR), superpixel segmentation, and a custom CNN (RadRGB), with 2814 RGB images and 1997 NIR.

While our model focused on banana disease classification, Ridhovan et al. (2022) used the DenseNet architecture to detect various banana leaf diseases (excluding *Fusarium*) and reported 84.73% accuracy. In a study closer to our scope, Zhang et al. (2022) utilized machine learning (Random Forest) on 570 banana images with the same type of sensor, reaching 97.28% accuracy, demonstrating the effectiveness of traditional ML models in specific contexts with well-structured data.

Furthermore, Sangeetha et al. (2023) assessed disease severity using image-based color and shape changes in banana leaves, achieving 91.56% accuracy, along with high precision (91.61%) and recall (88.56%). These higher values suggest that feature-based analysis and severity assessment can enhance model sensitivity.

As noted, incorporating larger and more diverse datasets, applying data augmentation, and exploring advanced architectures can further improve performance. Furthermore, improving *Fusarium* class recovery is crucial for early intervention and disease management in banana crops.

In addition to being used for classification models, the semantic segmentation technique can also be used for early disease detection. In their study, Elinisa et al. (2025) used a large set of images of banana plant diseases captured by a cell phone camera from 10 to 50 cm. For detection, they adopted the U-net network and obtained good results, achieving a Dice Coefficient of 96.45% and an Intersection over Union (IoU) of 93.23%.

In relation to the (i) set, evolution of accuracy (Figure 6a) it stabilizes between 5 and 10 epochs, with test accuracy slightly lower than training accuracy and with more oscillations but varying between 0.8 and 0.9. The evolution of loss (Figure 7a) shows a decrease in loss between 5 and 10 epochs (but stabilizes after 20 epochs. As shown in Figure 6a, between epochs 5 and 10, the training accuracy continues to improve, while the test accuracy plateaus, suggesting a divergence in performance. A similar pattern is observed in Figure 7a, in which the training loss consistently decreases, but the validation loss begins to increase after epoch 20, further indicating potential overfitting. This behaviour may be attributed to the limited size of the dataset, which restricts the model's ability to generalize effectively to unseen data.

To (ii) set, the training accuracy (Figure 6b) exhibits a steady increase (blue line), reaching values close to 1, while the validation accuracy (orange line) shows a similar pattern, although the values are slightly lower. The oscillations observed in the validation accuracy curve, especially in the first 20 epochs, may indicate less consistent learning in relation to the model's generalization, but the general trend is still one of improvement, highlighting the model's potential to classify

This contribution has been peer-reviewed. The double-blind peer-review was conducted on the basis of the full paper.
https://doi.org/10.5194/isprs-annals-X-3-W4-2025-371-2026 | © Author(s) 2026. CC BY 4.0 License.

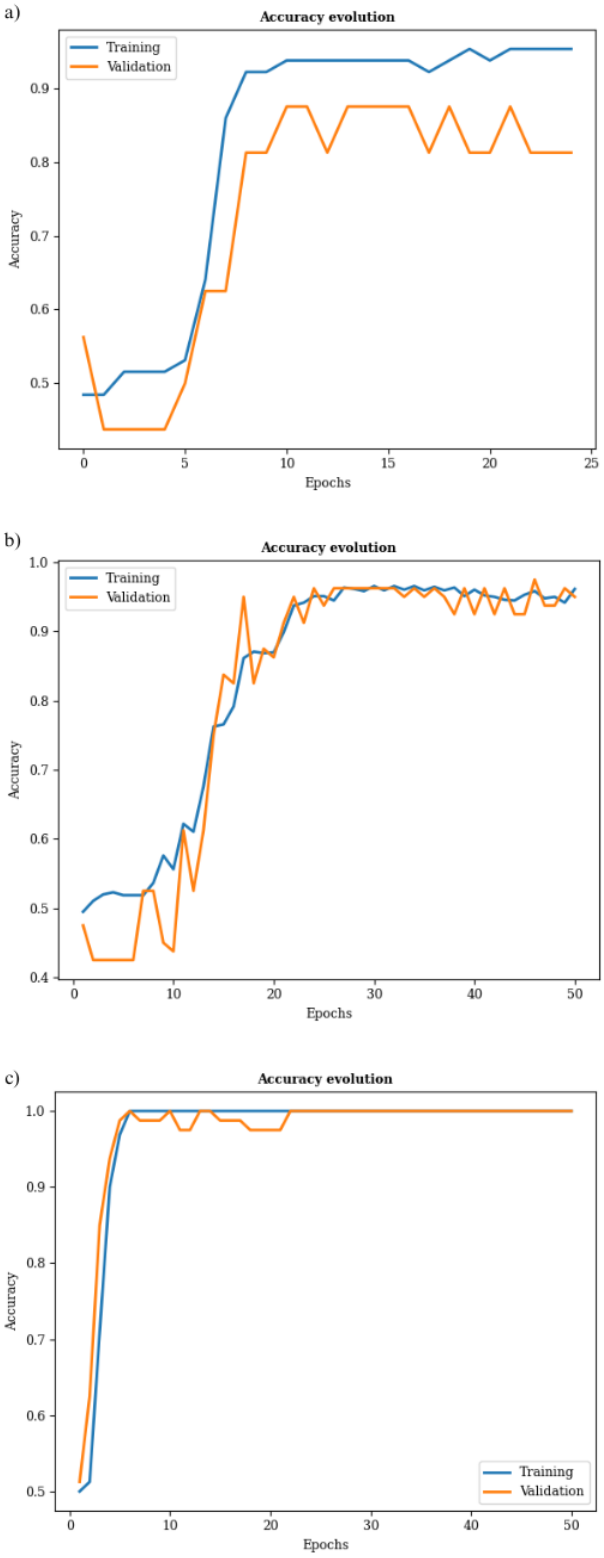

Figure 6. Training and validation accuracy at different times, showing the improvement in model performance and generalization ability over time, a) being the set (i), b) (ii) and c) (iii).

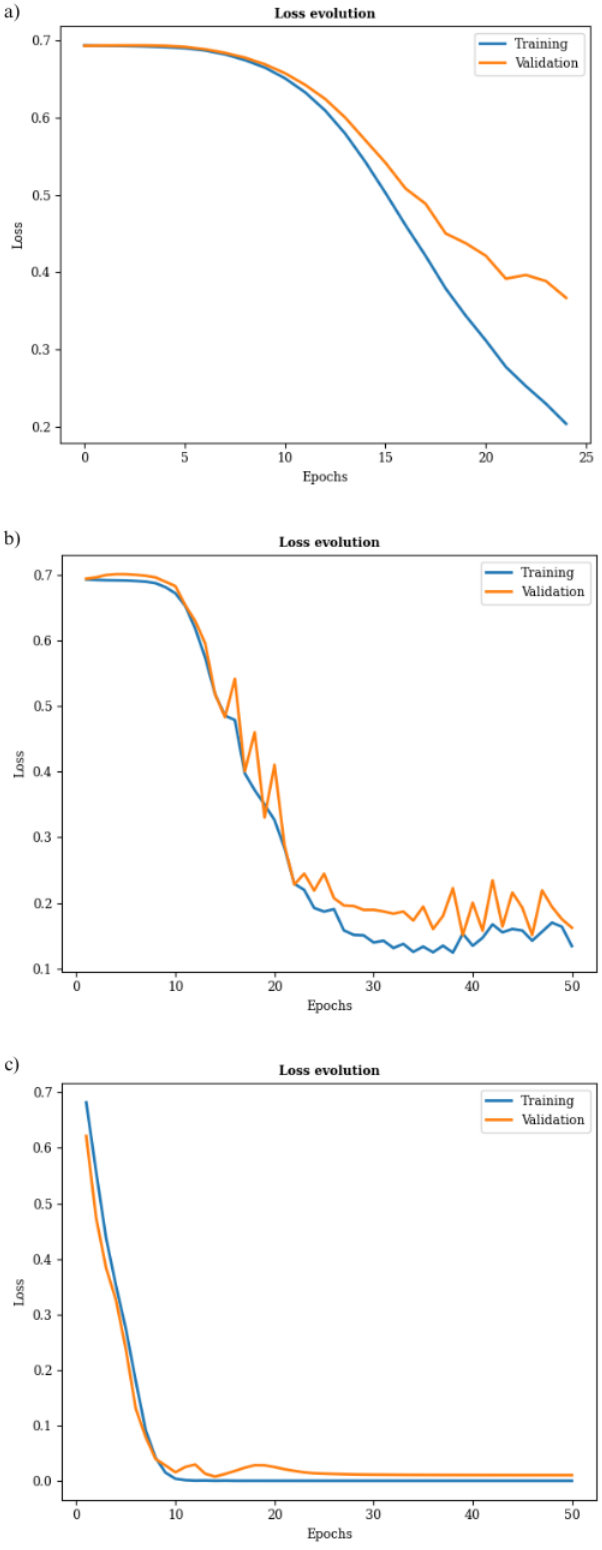

Figure 7. Training and validation loss over epochs, illustrating the model's learning progression and potential overfitting behaviour, a) being the set (i), b) (ii) and c) (iii).

diseases correctly. In Figure 7b, we can observe the loss trajectory across epochs for the training and validation sets. The training loss curve (blue line) demonstrates a continuous and stable decrease, suggesting that the model is effectively learning from the training data. On the other hand, the validation loss curve (orange line) also shows a decrease, but with a slight oscillation in the initial epochs, indicating a possible variation in the model's generalization. Notably, the validation loss does not show a significant increase, suggesting that the model is not suffering from significant overfitting, even though the

This contribution has been peer-reviewed. The double-blind peer-review was conducted on the basis of the full paper.
https://doi.org/10.5194/isprs-annals-X-3-W4-2025-371-2026 | © Author(s) 2026. CC BY 4.0 License.

validation loss remains slightly higher than the training loss.

To (iii) set, the training accuracy (Figure 6c) demonstrates a steady increase, quickly reaching values close to 1, indicating excellent performance in correctly classifying the training samples. The validation accuracy follows a similar pattern, with values also stabilizing at very high levels. This similarity suggests that the model generalized well, minimizing the risk of overfitting. The loss curve (Figure 7c) demonstrates a rapid decline in the first training cycles, with the loss curves for the training set (blue line) and validation set (orange line) converging and stabilizing at very low values after approximately 10 epochs. The slight oscillation observed in the first epochs may indicate natural fluctuations during the initial learning phase, but it did not compromise overall performance.

The confusion matrix shown in Figure 8 illustrates the performance of the model on a binary classification task. In Figure 8a, the model demonstrates perfect classification for class 0 "*Healthy*", with all 7 instances correctly identified. For class 1 "*Fusarium*", 6 instances were correctly classified, while 3 were misclassified as class 0 "*Healthy*". This asymmetry indicates that the model is more effective at recognizing class 0 than class 1. Although the overall precision reaches 1.00, indicating that all positive predictions made by the model were correct, the overall recall is 0.67, suggesting that one-third of actual positive cases (class 1) were not detected. This highlights a trade-off between precision and recall, and suggests the model may benefit from further tuning or additional data to improve sensitivity toward class 1.

This is confirmed in Figure 8b, in which techniques were implemented to improve the model (ii). The model correctly classified 39 samples as "*Healthy*," and only 1 sample was incorrectly classified as "*Healthy*" when it was "*Fusarium*" (false positive). The model misclassified 3 samples as "*Fusarium*" when they should have been identified as "*Healthy*" (false negatives). These numbers reveal that the model performs quite well, with a high rate of true positives and true negatives. The number of false positives and false negatives is relatively low, indicating that the model is effective in discriminating between the two classes. For iii, all classes were correctly identified, indicating the model's excellence.

4. Conclusion

The results show that the CNN was able to identify plants infected by *Fusarium oxysporum*, contributing to automated disease detection, reducing the need for manual inspection, and optimizing agricultural management. Despite the small sample size, the network performed well, but improvements were still needed in model accuracy, especially for recall, where visualization of the disease is necessary to extract the plant. Data augmentation and k-fold performed very well. But when other techniques (such as segmentation based on vegetation indices, class weight and callbacks) were applied to mitigate overfitting caused by the scarcity of samples, the network performed excellently, with maximum results for the metrics. As a future perspective, it is proposed to implement the developed CNN in another application area, allowing to verify the model's generalization capacity in different contexts.

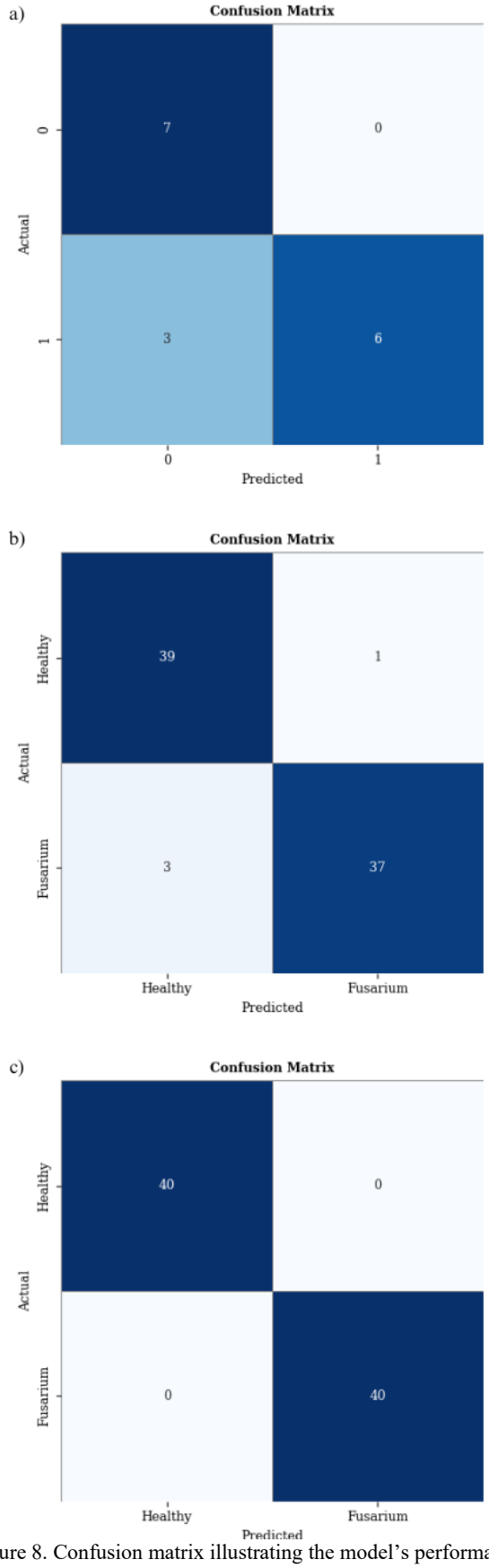

Figure 8. Confusion matrix illustrating the model's performance on the binary classification task to each set – a) i, b) ii and c) iii. The matrix shows the number of correct and incorrect predictions for each class, where (0) it`s "healthy" class and (1) "*Fusarium*" class.

This contribution has been peer-reviewed. The double-blind peer-review was conducted on the basis of the full paper.
https://doi.org/10.5194/isprs-annals-X-3-W4-2025-371-2026 | © Author(s) 2026. CC BY 4.0 License.

Acknowledgements

I would like to thank FCT/UNESP (Brazil)for all the structure provided and UFPR (Brazil) for the support given through Professor Hideo for the development of this work. This study was financed in part by the Coordenação de Aperfeiçoamento de Pessoal de Nível Superior – Brazil (CAPES) (Grant: 88887.807669/2023-00), and by the São Paulo Research Foundation, FAPESP (Grant: 2021/06029-7).

Data Availability Statement

The data set used in evaluating the trained neural network is accessible via the following link: https://cstr.cn/31253.11.sciencedb.07000 (accessed on 17 May 2025), made available by Science Data Bank.

References

Brazilian Agricultural Research Corporation (EMBRAPA). Fusarium blight of banana. 2022. https://www.infoteca.cnptia.embrapa.br/infoteca/bitstream/doc/1142635/1/FolderBioinsumos-Augusto-Leandro-2022-AINFO.pdf (25 April 2025).

Chen, Junde, Chen, Jinxiu, Zhang, D., Sun, Y., Nanehkaran, Y.A., 2020. Using deep transfer learning for image-based plant disease identification. *Computers and Electronics in Agriculture* 173, 105393. https://doi.org/10.1016/j.compag.2020.105393

Couteaudier, Y., C. Alabouvette. Fusarium wilt diseases in soilless cultures. *Symposium on Substrates in Horticulture other than Soils In Situ 126*. 1981.

Dang, L.M., Ibrahim Hassan, S., Suhyeon, I., Sangaiah, A. kumar, Mehmood, I., Rho, S., Seo, S., Moon, H., 2020a. UAV based wilt detection system via convolutional neural networks. S*ustainable Computing: Informatics and Systems* 28, 100250. https://doi.org/10.1016/j.suscom.2018.05.010

Dang, L.M., Wang, H., Li, Y., Min, K., Kwak, J.T., Lee, O.N., Park, H., Moon, H., 2020b. Fusarium Wilt of Radish Detection Using RGB and Near Infrared Images from Unmanned Aerial Vehicles. *Remote Sensing* 12, 2863. https://doi.org/10.3390/rs12172863

Denny, Y.R., Permata, E., Assaat, L.D., 2022. Classification of Diseases of Banana plant Fusarium Wilted Banana Leaf Using Support Vector Machine. *Gravity: Jurnal Ilmiah Penelitian dan Pembelajaran Fisika* 8. https://doi.org/10.30870/gravity.v8i1.15893

Elinisa, C.A., Wa Maina, Ciira, Vodacek, Anthony, and Mduma, N., 2025. Image Segmentation Deep Learning Model for Early Detection of Banana Diseases. *Applied Artificial Intelligence* 39, 2440837. https://doi.org/10.1080/08839514.2024.2440837

Fall, A.L., Byrne, P.F., Jung, G., Coyne, D.P., Brick, M.A., Schwartz, H.F., 2001. Detection and Mapping of a Major Locus for Fusarium Wilt Resistance in Common Bean. *Crop Science* 41, 1494–1498. https://doi.org/10.2135/cropsci2001.4151494x

FAOSTAT. Countries by commodity (2023). https://www.fao.org/faostat/en/#rankings/countries_by_commodity (17 May 2025).

Gitelson, A.A., Kaufman, Y.J., Merzlyak, M.N., 1996. Use of a green channel in remote sensing of global vegetation from EOS-MODIS. *Remote Sensing of Environment* 58, 289–298. https://doi.org/10.1016/S0034-4257(96)00072-7

Gitelson, A.A., Merzlyak, M.N., 1996. Signature Analysis of Leaf Reflectance Spectra: Algorithm Development for Remote Sensing of Chlorophyll. *Journal of Plant Physiology* 148, 494–500. https://doi.org/10.1016/S0176-1617(96)80284-7

LeCun, Y., Boser, B., Denker, J.S., Henderson, D., Howard, R.E., Hubbard, W., Jackel, L.D., 1989. Backpropagation Applied to Handwritten Zip Code Recognition. *Neural Computation* 1, 541–551. https://doi.org/10.1162/neco.1989.1.4.541

Lin, S., Ji, T., Wang, J., Li, K., Lu, F., Ma, C., Gao, Z., 2025. Bfwsd: A Lightweight Algorithm for Rapid Assessment of Banana Fusarium Wilt in Large Areas. *SSRN*. https://doi.org/10.2139/ssrn.5210638

Nakkeeran, S., Rajamanickam, S., Saravanan, R., Vanthana, M., Soorianathasundaram, K., 2021. Bacterial endophytome-mediated resistance in banana for the management of Fusarium wilt. 3 *Biotech* 11, 267. https://doi.org/10.1007/s13205-021-02833-5

Pegg, K.G., Coates, L.M., O'Neill, W.T., Turner, D.W., 2019. The Epidemiology of Fusarium Wilt of Banana. *Front. Plant Sci*. 10. https://doi.org/10.3389/fpls.2019.01395

Ploetz, R.C., 2021. Gone Bananas? Current and Future Impact of Fusarium Wilt on Production, in: Scott, P., Strange, R., Korsten, L., Gullino, M.L. (Eds.), Plant Diseases and Food Security in the 21st Century. *Springer International Publishing*, Cham, pp. 21–32. https://doi.org/10.1007/978-3-030-57899-2_2

Ploetz, R.C., 2015. Fusarium Wilt of Banana. Phytopathology® 105, 1512–1521. https://doi.org/10.1094/PHYTO-04-15-0101-RVW

Ridhovan, A., Suharso, A., Rozikin, C., 2022. Disease Detection in Banana Leaf Plants using DenseNet and Inception Method. *Jurnal RESTI (Rekayasa Sistem dan Teknologi Informasi)* 6, 710–718. https://doi.org/10.29207/resti.v6i5.4202

Rouse, J.W., Haas, R.H., Schell, J.A., Deering, D.W., 1974. Monitoring vegetation systems in the Great Plains with ERTS. Sanga, S., Mero, V., Machuve, D., Mwanganda, D., 2020.

Sanga, S., Mero, V., Machuve, D., Mwanganda, D., 2020. Mobile-Based Deep Learning Models for Banana Diseases Detection. *Paper presented at the ICLR 2020 Workshop on Computer Vision for Agriculture.* https://doi.org/10.48550/arXiv.2004.03718

Sangeetha, R., Logeshwaran, J., Rocher, J., Lloret, J., 2023. An Improved Agro Deep Learning Model for Detection of Panama Wilts Disease in Banana Leaves. *AgriEngineering* 5, 660–679. https://doi.org/10.3390/agriengineering5020042

Simmonds, N. W, 1966. *Bananas*. Longman, London.

Stover, R.H., 1962. *Fusarial Wilt (Panama Disease) of Bananas and Other Musa Species*. Commonwealth Mycological Institute.

Stover, R. H., Waite, B. H. (1954). Colonization of banana roots by *Fusarium oxysporum* f. *cubense* and other soil fungi. *Phytopathology* 44, 689–693.

Yadav, R.K., Tripathi, M.K., Tiwari, S., Tripathi, N., Asati, R., Patel, V., Sikarwar, R.S., Payasi, D.K., 2023. Breeding and Genomic Approaches towards Development of Fusarium Wilt Resistance in Chickpea. *Life* 13, 988. https://doi.org/10.3390/life13040988

Yan, K., Shisher, M.K.C., Sun, Y., 2023. A Transfer Learning-Based Deep Convolutional Neural Network for Detection of Fusarium Wilt in Banana Crops. *AgriEngineering* 5, 2381–2394. https://doi.org/10.3390/agriengineering5040146

Ye, H., Chen, S., Guo, A., Nie, C., Wang, J., 2023. A dataset of UAV multispectral images for banana Fusarium wilt survey. https://doi.org/10.57760/sciencedb.07000

Ye, H., Huang, W., Huang, S., Cui, B., Dong, Y., Guo, A., Ren, Y., Jin, Y., 2020a. Identification of banana fusarium wilt using supervised classification algorithms with UAV-based multi-spectral imagery. *International Journal of Agricultural and Biological Engineering* 13, 136–142. https://doi.org/10.25165/ijabe.v13i3.5524

Ye, H., Huang, W., Huang, S., Cui, B., Dong, Y., Guo, A., Ren, Y., Jin, Y., 2020b. Recognition of Banana Fusarium Wilt Based on UAV Remote Sensing. *Remote Sensing* 12, 938. https://doi.org/10.3390/rs12060938

Zhang, S., Li, X., Ba, Y., Lyu, X., Zhang, M., Li, M., 2022. Banana Fusarium Wilt Disease Detection by Supervised and Unsupervised Methods from UAV-Based Multispectral Imagery. *Remote Sensing* 14, 1231. https://doi.org/10.3390/rs14051231

Zhu, Y., Abdelraheem, A., Lujan, P., Idowu, J., Sullivan, P., Nichols, R., Wedegaertner, T., Zhang, J., 2021. Detection and Characterization of Fusarium Wilt (Fusarium oxysporum f. sp. vasinfectum) Race 4 Causing Fusarium Wilt of Cotton Seedlings in New Mexico. *Plant Disease* 105, 3353–3367. https://doi.org/10.1094/PDIS-10-20-2174-RE